

# THREE DIMENSIONAL SCALABLE ALL-SPEED CFD CODE GASFLOW-MPI: APPLICATIONS TO TURBULENT COMBUSTION OF PREMIXED HYDROGEN-AIR MIXTURES WITH HEAT AND MASS TRANSFER

Jianjun Xiao<sup>a</sup>, John R. Travis<sup>b</sup>, Reinhard Redlinger<sup>a</sup>, Mike Kuznetsov<sup>a</sup>,  
Anatoly Svishchev<sup>a</sup>, Wolfgang Breitung<sup>a</sup> and Thomas Jordan<sup>a</sup>

<sup>a</sup>Institute of Nuclear and Energy Technologies,  
Karlsruhe Institute of Technology,  
Hermann-von-Helmholtz-Platz 1, 76344 Eggenstein-Leopoldshafen, Germany  
jianjun.xiao@kit.edu; reinhard.redlinger@kit.edu; mike.kuznetsov@kit.edu; anatoly.svishchev@kit.edu;  
breitung@simaps.de; thomas.jordan@kit.edu  
<sup>b</sup>Engineering and Scientific Software Inc.,  
Santa Fe, New Mexico 87505, U.S.A.  
jack\_travis@comcast.net

## ABSTRACT

It is well known that the risk of hydrogen combustion has become one of the key safety issues for the further evolution of nuclear power plants (NPP) especially after energetic hydrogen explosions occurred at units No. 1, No. 3 and No. 4 in the Fukushima Daiichi nuclear disaster in 2011. Complex physics phenomena are involved in NPP containments during a postulated severe accident, such as steam condensation and evaporation, heat conduction in solid structures, convective heat transfer, radiation heat transfer, turbulent flow, flashing of water, behavior of spray droplets, draining water film, hydrogen deflagration and detonation, hydrogen mitigation measures, aerosol and fission product behavior and so on. A high performance fully validated best-estimate tool is highly desired to accurately predict these phenomena in complex accident sequences. GASFLOW-MPI solves 3-D transient, two-phase, compressible Navier-Stokes equations for multi-species using a proven algorithm of Implicit Continuous Eulerian-Arbitrary Lagrangian-Eulerian (ICE'd-ALE) methodology for all-speed flows. The objective is to achieve seamless comprehensive simulations of major physics phenomena in the containment using the high-performance, scalable CFD code GASFLOW-MPI. The code has been applied to SARNET 2 hydrogen fast deflagration experimental data from the ENACCEF facility. The effects of blockage ratio, diluents, steam condensation, convective and radiation heat transfer were studied. It indicates that flame propagation of the deflagration, pressure increase rates and peak pressures in the obstructed tube can be well predicted by GASFLOW-MPI. Further validation work will be performed for the recently extended combustion models and conjugate heat transfer models in the GASFLOW-MPI code in the future.

## KEYWORDS

GASFLOW-MPI, CFD, ENACCEF, nuclear power plant (NPP), containment

## 1. INTRODUCTION

During a postulated severe accident, complex coupled physics phenomena are involved in the NPP containment, such as flashing of water, turbulent flow, convective heat transfer, radiation heat transfer, steam condensation and evaporation, heat conduction in solid structure, hydrogen deflagration and detonation, buoyancy-driven flow, heat and mass exchange of the spray droplets, draining thin water film, hydrogen ignition and recombination, aerosol and fission product transportation and decay, and so on [1]. In order to investigate and control the hydrogen explosion risk, it is of high significance to accurately simulate all these coupled complicated physical phenomena in large scale containments with reasonable

computational effort which requires a high performance, fully validated and parallelized computer code [2].

GASFLOW is a CFD code used to simulate fluid dynamics, heat and mass transfer, chemical reaction, aerosol transportation and other related physics phenomena in geometrically complex domains, such as a nuclear reactor containment during a postulated severe accident [3-4]. GASFLOW solves 3-D transient, compressible Navier-Stokes equations for multi-species using a proven pressure-based algorithm of ICE'd-ALE methodology for all-speed flows [5-6]. In the past decades, GASFLOW has been extensively validated and applied to the simulation of hydrogen and steam distributions in the nuclear reactor containments [7-30]. These calculation results have been well accepted by the nuclear authorities of several European and Asian countries. However, the users have often suffered from the extremely long computational time, which is due to the fact that GASFLOW was designed as a sequential code which could be executed principally on vector supercomputer machines using only one single processor. Simulations of deflagration and detonation involve more detailed physics and require smaller scales of time and space, which takes considerably larger computational efforts. Therefore, during the past decades only simple combustion models using Arrhenius Global Chemical Kinetics relationships were available in the GASFLOW sequential version.

The new GASFLOW-MPI code [31] is developed by the authors at Karlsruhe Institute of Technology. It is the parallel version of GASFLOW. GASFLOW-MPI employs the paradigms of message passing and domain decomposition based on the PETSc library and can be run on any kind of parallel systems which support Message Passing Interface (MPI). With the high performance computing capability now enabled by GASFLOW-MPI, simulations of more complex physical phenomena with more geometric details are becoming feasible. Recently, the number of GASFLOW users who request the improvement and extension of the combustion models in GASFLOW-MPI has been increasing, including Areva GmbH, Tsinghua University and Shanghai Jiaotong University. Another GASFLOW user, KAERI, has tried to interface GASFLOW distribution simulations with OpenFOAM combustion simulations [24]. Historically speaking, the pressure-based algorithm was originally developed for low Mach number flows or incompressible flows, while the density-based approach was usually applicable to high-speed compressible flows. Both approaches have been extended beyond their original intent for wider flow regimes since the 1970's. However, during the past decades the nuclear safety engineers have been using the pressure-based implicit solvers for hydrogen distribution simulations and the density-based explicit solvers for hydrogen combustion simulations [30]. When information is transferred between two different codes, extra effort of special data manipulations is required, and the consistency of field properties and geometry details may not be maintained. Therefore, it is desperately needed by the nuclear safety engineers to have one integrated, robust, scalable and efficient computing platform to compute the entire accident scenario in a transparent and convenient way. Thanks to the robust ICE'd ALE algorithm for all-speed flows, the GASFLOW-MPI code is not only applicable to flow regimes of slow speed, such as mixing, slow deflagration and buoyancy driven flow, but also valid for high-speed, combustion-driven compressible flows [5-6, 31].

The objective is to achieve seamless simulations of the complicated coupled physical phenomena in geometrically complex NPP containment, such as thermal hydraulics, chemical kinetics, aerosol transportation, fission product decay, hydrogen mitigation and so on, using the high performance pressure-based semi-implicit CFD code GASFLOW-MPI. In order to accommodate for significantly different time steps of combustion simulations and distribution simulations, a special criteria has been introduced in the code. It controls the time step depending on the regimes of flow and combustion. This methodology requires no data manipulation, which is usually needed in order to simulate those different flow and combustion regimes. It automatically keeps consistency of the data throughout the calculation. The combustion models based on the solution of the transportation of the density-weighted mean reaction progress variable has been developed in GASFLOW-MPI in order to simulate turbulent flame

propagation. In order to validate the extended combustion models in GASFLOW-MPI, the calculation results were compared with the SARNET-2 hydrogen deflagration experiments performed in the ENACCEF facility [32].

The governing equations, numerical algorithm and combustion models in GASFLOW-MPI are introduced in Section 2. Section 3 briefly introduces the hydrogen deflagration experiments performed in the ENACCEF facility. The calculation results are compared to the experimental data in Section 4. In Section 5, the main findings are discussed and future code development work is explained.

## 2. PARALLEL CFD CODE GASFLOW-MPI

### 2.1. Governing equations and numerical algorithm

The governing equations of volume, mass, momentum and internal energy in GASFLOW-MPI can be written as

$$\begin{cases} \frac{d}{dt} \int_V dV = \oint_S (\mathbf{b} - \mathbf{u}) \cdot \mathbf{A} dS + \int_V S_V dV \\ \frac{d}{dt} \int_V \rho_\alpha dV = \oint_S [\rho_\alpha (\mathbf{b} - \mathbf{u}) \cdot \mathbf{A} + (\mathbf{J}_\alpha \cdot \mathbf{A})] dS + \int_V S_{\rho,\alpha} dV; \alpha = 1, N \\ \frac{d}{dt} \int_V \rho \mathbf{u} dV = \oint_S [\rho \mathbf{u} (\mathbf{b} - \mathbf{u}) \cdot \mathbf{A} - p - (\boldsymbol{\tau} \cdot \mathbf{A}) - (\mathbf{D}_d \cdot \mathbf{A})] dS + \int_V (\rho \mathbf{g} + \mathbf{S}_m) dV \\ \frac{d}{dt} \int_V \rho I dV = \oint_S [\rho I (\mathbf{b} - \mathbf{u}) \cdot \mathbf{A} - p (\mathbf{u} \cdot \mathbf{A}) + (\mathbf{q} \cdot \mathbf{A})] dS + \int_V S_I dV \end{cases} \quad (1)$$

where  $\mathbf{b}$  is the velocity of the control surface  $S$ ,  $\mathbf{u}$  is the velocity of the fluid, and  $\mathbf{A}$  is the outward normal fractional area vector.  $\mathbf{J}_\alpha \cdot \mathbf{A}$  is the mass diffusion flux vector.  $\mathbf{D}_d \cdot \mathbf{A}$  is the internal structure drag vector.  $\mathbf{q} \cdot \mathbf{A}$  is the Internal energy flux vector.  $S_V$ ,  $S_{\rho,\alpha}$ ,  $S_m$  and  $S_I$  are the source terms of volume, species, momentum and internal energy. ICE'd ALE is applicable to flows at all speeds, meaning from supersonic to the incompressible limit. It is time-split into three distinct phases: Phase A: An explicit Lagrangian phase where the diffusion terms and source terms are solved; Phase B: An implicit Lagrangian phase where pressure waves are propagated without time-step restrictions; Phase C: An explicit convection phase.

### 2.3. Combustion models in GASFLOW-MPI

To model the flame front propagation, the transport equation of the density-weighted mean reaction progress variable is solved

$$\frac{\partial}{\partial t} (\rho \xi) + \nabla \cdot (\rho \xi \mathbf{u}) = \nabla \cdot \left[ \left( \rho \mathbf{v} + \frac{\mu_t}{Sc_t} \right) \nabla \xi \right] + \rho S_\xi \quad (2)$$

The combustion progress variable,  $\xi$ , is usually written

$$\xi(\mathbf{x}, t) = \frac{Y_{H_2}(\mathbf{x}, t) - Y_{H_2, initial}(\mathbf{x}, t)}{Y_{H_2, final}(\mathbf{x}, t) - Y_{H_2, initial}(\mathbf{x}, t)} \quad (3)$$

with the progress variable being either 1 in the burnt mixture or 0 in the unburnt mixture. The key to this modeling approach is the source term,  $\rho S_\xi$ . Some of the source term models which have been implemented in GASFLOW-MPI are outlined below.

#### 2.3.1. Arrhenius Rate

Although indirectly turbulence is accounted for through turbulent diffusion in Equation (2), this approach directly neglects the effect of turbulence. It assumes that chemistry plays the most important role in the combustion process. In GASFLOW-MPI, the reaction rate is given by [34] as

$$\rho S_{\xi} = A_f \rho (1 - \xi) \exp\left(-\frac{E_a}{RT}\right) \quad (4)$$

### 2.3.2. Eddy Break-up Model (EBU)

This model is based on phenomenological analysis of turbulent combustion for high turbulent Reynolds number ( $Re_t = u'_t l_t / \nu$ ), which characterizes a turbulent flow in terms of the turbulent root mean square (RMS) velocity and turbulent integral length scale, and high Damkohler number ( $Da = \tau_t / \tau_c$ ), which is the ratio of the turbulent integral time scale,  $\tau_t$ , to the chemical time scale,  $\tau_c$ . The chemical kinetic rates are neglected and the mean reaction rate is mainly controlled by turbulent mixing time. In GASFLOW-MPI, The source term is given by [35] as

$$\rho S_{\xi} = -C_{EBU} \rho \frac{\varepsilon}{k} \xi (1 - \xi) \quad (5)$$

where  $C_{EBU}$  is a model constant.

### 2.3.3. Eddy Dissipation Model (EDM)

This model is based on the assumption that combustion occurs at small scales, where mixing occurs on a molecular level and the rate is assumed to be proportional to the inverse of the turbulent time scale. It was developed from the original eddy break-up model, the most significant difference being that the EDM model accounts for the fact that the reaction rate cannot occur unless both fuel and oxidizer mix on a molecular scale at a sufficient temperature. This is accomplished by relating the reaction rate to the limiting species. In GASFLOW-MPI, the model is formulated as follows [36]:

$$\rho S_{\xi} = B_1 \rho \frac{\varepsilon}{k} \min\left(Y_{H_2}, \frac{Y_{O_2}}{\phi}, B_2 \frac{Y_{H_2O}}{1 + \phi}\right) \quad (6)$$

where  $B_1$  and  $B_2$  are model constants, and  $\phi$  is the equivalence ratio.

### 2.3.4. Peters G-equation approach

Using the level set approach, Peters [37] derived an averaged G-equation instead of the combustion progress variable,  $\xi$ , to track flame propagation. In GASFLOW-MPI, the averaged G-equation can be written

$$\frac{\partial}{\partial t}(\rho G) + \nabla \cdot (\rho G \mathbf{u}) = \mu_t |\nabla G| \nabla \cdot \left( \frac{\nabla G}{|\nabla G|} \right) + \rho S_t |\nabla G| \quad (7)$$

where the turbulent flame speed,  $S_t$ , is given by

$$S_t = S_L \left\{ 1 - \frac{0.39}{2} \frac{l_t}{l_F} + \left[ \left( \frac{0.39}{2} \frac{l_t}{l_F} \right)^2 + 0.78 \frac{u'_t}{S_L} \frac{l_t}{l_F} \right]^{\frac{1}{2}} \right\} \quad (8)$$

### 2.3.5. Zimont Model

Zimont [38-39] proposed that turbulent premixed flames can be modeled by solving the combustion progress variable Equation (2), where the source term is given by

$$\rho S_{\xi} = -\nabla \cdot [\rho \mathcal{V} \xi] + \rho_u S_T |\nabla \xi| \quad (9)$$

In GASFLOW-MPI, the Zimont turbulent flame speed closure is calculated by a model for wrinkled and thickened flame fronts [40]

$$S_T = A(u_i') Da^{1/4} = A(u_i')^{3/4} S_L^{1/2} \alpha^{-1/4} l_t^{1/4} \quad (10)$$

where the model constant  $A = 0.52$  which is suitable for most of the premixed flames,  $S_L$  is the laminar flame speed,  $\alpha = k/\rho c_p$  is thermal diffusivity of unburnt mixture, and  $l_t$  is the turbulent length scale which is calculated by

$$l_t = C_D (u')^3 / \varepsilon \quad (11)$$

where  $C_D$  is the constant value (0.09) used in  $\kappa$ - $\varepsilon$  model,  $u'$  is the turbulent velocity fluctuation and  $\varepsilon$  is the turbulent dissipation rate.

It should be noted that the Zimont combustion model evaluates flame propagation of completely developed turbulent flames. Laminar flame propagation, transition from laminar flames to turbulent flames and ignition modeling are not accounted for. Some of the drawbacks of the Zimont combustion model can be improved by Lipatnikov combustion model [41].

### 2.3.6. Kawanabe Model

There has been considerable effort to obtain accurate correlations for the turbulent burning velocity  $S_T$ . One of the more simple relationships is due to Kawanabe, et al. and implemented in GASFLOW-MPI by

$$S_T = S_L \left[ 1 + 1.25 \left( \frac{u_i'}{S_L} \right)^{0.7} \right] \quad (12)$$

### 2.3.7. Schmid Model

Another of the more simple relationships was developed by Schmid, et al. [42], and implemented in GASFLOW-MPI as

$$S_T = S_L \left[ 1 + \left( \frac{u_i'}{S_L} \right) \left( 1 + \frac{1}{Da^2} \right)^{-1/4} \right] \quad (13)$$

## 3. ENACCEF FACILITY FOR HYDROGEN DEFLAGRATION EXPERIMENTS

ENACCEF is a vertical facility about 5 m long, which is divided in two parts, as illustrated in Figure 1. The first part is the acceleration tube, which contains annular flow obstacles with constant separation and blockage ratio. The obstacle positions are 0.622 m, 0.776 m, 0.93 m, 1.084 m, 1.238 m, 1.392 m, 1.546 m, 1.7 m and 1.89 m. The tube is 3.2 m long and its internal diameter is 154 mm. The tube is equipped with two low energy ignition devices at its bottom-end. At a distance of 1.9 m from the ignition point, 3 rectangular quartz windows are mounted which allow the recording of the flame front during its propagation along the tube. The tube is also equipped with 11 small quartz windows. The dome is 1.7 m long with the internal diameter of 738 mm. It is connected to the upper part of the acceleration tube via a flange. This part of the facility is also equipped with 3 silica windows through which the arrival of the flame can be recorded.

Two experimental campaigns have been conducted. All tests were performed under the conditions of temperature = 23°C and pressure = 1 bar. The ignition point is located 138 mm from the bottom of the facility, and the ignition energy delivered was estimated as 100 mJ. To investigate the effect of turbulence on the flame propagation, two tests were performed with the same initial gas mixture (13 vol.% H<sub>2</sub> and 87 vol.% air) and various blockage ratios, BR=0.33 (RUN 158) and BR=0.63 (RUN153). The objective of the second campaign was to study the effect of diluents on flame propagation. The diluent is composed by of 60 vol.% CO<sub>2</sub> and 40 vol.% He, which serves as a simulant for steam. Three tests were conducted with the same geometrical configuration of BR=0.63. The initial gas mixtures were 13 vol.% H<sub>2</sub> + 77 vol.% air + 10 vol.% diluents (TEST 1), 13 vol.% H<sub>2</sub> + 67 vol.% air + 20 vol.% diluents (TEST 2) and 13 vol.% H<sub>2</sub> + 57 vol.% air + 30 vol.% diluents (TEST 3).

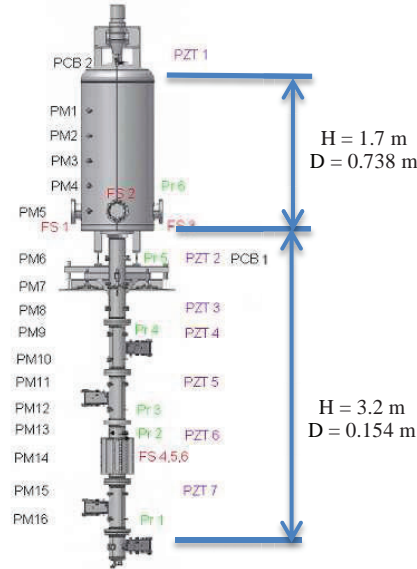


Figure 1. ENACCEF instrumentation

#### 4. CALCULATION RESULTS OF GASFLOW-MPI

The main purpose is to study the effects of blockage ratio (cases 1-2), various mechanisms of heat transfer (cases 3-7) and diluents (cases 8-10). More details of these ten testing cases are shown in Table 1. The axisymmetric computational domain was generated in the cylindrical coordinate. Mesh sensitivity analysis was also performed. The numbers of cells in radial, azimuthal and axial direction are 33, 1 and 313, respectively. The mesh was locally refined near the wall. Heat transfer inside the wall of the tube was simulated with 51 radial nodes. The thermal conductivity used in the heat conduction simulation is 50 W/mK, and the specific heat capacity is 0.4904 J/gK.

Table 1. Testing cases for GASFLOW-MPI simulations

Case	Test name	Blockage ratio (BR)	H <sub>2</sub>	Air	diluents	Convective heat transfer	Radiation heat transfer	Steam condensation
<b>Effect of turbulence</b>								
1	RUN 153	0.63	13%	87%	0	on	on	on
2	RUN 158	0.33	13%	87%	0	on	on	on
<b>Effect of heat transfer modeling</b>								
3	RUN 153	0.63	13%	87%	0	on	off	on
4	RUN 153	0.63	13%	87%	0	off	on	on
5	RUN 153	0.63	13%	87%	0	off	off	off
6	RUN 153	0.63	13%	87%	0	on	on	off
7	RUN 158	0.33	13%	87%	0	off	off	off
<b>Effect of diluents</b>								
8	TEST 1	0.63	13%	77%	10%	on	on	on
9	TEST 2	0.63	13%	67%	20%	on	on	on
10	TEST 3	0.63	13%	57%	30%	on	on	on

The simulations were initiated with a hydrogen molar fraction of 13%, a pressure of 1.0 bar and a temperature of 296 K. The walls were modeled as no-slip boundaries with either an initial temperature of 296 K for heat transfer or adiabatic heat transfer. The material used for heat conduction simulation was steel, and the emissivity for thermal radiation modeling was assumed to be constant at 0.5 in the simulation. The  $\kappa$ - $\epsilon$  turbulence model was adopted. Very weak initial turbulent kinetic energy ( $1.0 \text{ g}\cdot\text{cm}^2/\text{s}^2$ ) and dissipation ( $1.0 \text{ cm}^2/\text{s}^3$ ) were used in order to approach the timing of the flame acceleration. The hydrogen combustion was modeled using the burning velocity model with the Zimont turbulent flame speed closure in GASFLOW-MPI. The simulations were carried out using second order Van Leer scheme in space. The convergence criteria of linear solvers for pressure elliptic equation and radiation equation were both  $1.0\text{e-}6$ .

#### 4.1. Effect of turbulence and heat transfer on the flame propagation

The experimental data of RUN 153 and computed pressure time evolutions at the PCB1 pressure transducer, which was located at the end of the acceleration tube, are shown in Figure 1. The first pressure peak of around 2.5 bar was measured at time 0.109 s, which is due to the pre-cursor wave traveling along the tube in front of the accelerating flame. This leading pressure wave in the unburned gas is captured by GASFLOW-MPI in all the cases as shown in Figure 2. The measured maximum pressure value was 4.98 bars and the rate of pressure increase ( $dp/dt$ ) was around 142 bar/s. Compared to the experimental data, pressure increase rates were slightly over predicted at the PCB1 location in the cases of 1, 3, 4, 5 and 6, as shown in Figure 2 during 0.09-0.11 s. As in RUN 153 the best agreement with the measured pressures after flame arrival (0.1 -0.2 s) were obtained in the simulations with convective heat transfer (cases 1, 3 and 6 in Figure 2).

The effects of condensation, convective and radiation heat transfer on the pressure increase in RUN 153 are studied in cases 1, 3, 4, 5 and 6 in Figure 2. With condensation and thermal radiation switched on in cases 1, 4 and 6, there is roughly 0.01 s delay compared to cases 3 and 5 when the pressure starts to increase at the sensor PCB1. For case 5 in which the heat transfer was not modeled, the magnitude of the calculated pressure is higher than the measured pressure. For cases 1, 3 and 6 with convective heat transfer modeled, the pressure decay agrees well with the experimental data before 0.2 s. It seems that the convective heat transfer dominates the heat losses during 0.1 ~ 0.2 s in the GASFLOW-MPI simulation. The thermal radiation has only a small contribution to the pressure decrease before 0.2 s as observed from the results of case 4. Steam condensation modeling was switched off in case 6, and very small discrepancies were observed compared to cases 1 and 3. It means that the contribution of condensation to the overall heat loss is relatively small in the computed ENACCEF cases.

The effects of different heat loss mechanisms on the flame front position in the tube for cases 1, 3, 4 and 5 are shown in Figure 3. When the thermal radiation is modeled, such as cases 1 and 4, the flame front propagates with around 0.1 s delay compared to the results of case 3 and 5 in which thermal radiation is not considered. It indicates that the thermal radiation modeling has a noticeable impact on the flame front position during the run-up phase. In the acceleration phase, good agreement was obtained between the calculated results (case 1, 3, 4 and 5) and the experimental data. It means that the effect of heat transfer on the flame propagation during the flame acceleration phase is negligible.

The simulation results of pressure time evolutions and flame front position in RUN 158, which used the same gas mixture but a smaller blockage ratio (33%), are plotted in Figure 4 and Figure 5. The magnitude of the first pressure peak was well predicted by GASFLOW-MPI. The computed pressure increase rates when the flame arrives were slightly over predicted compared to the measured ones. After the combustion, the average pressure is around 5.1 bars without heat transfer modeling in case 7. In case 2 with convective, radiation and condensation heat transfer models, the average pressure is roughly 4.5 bars

which agree well with the experimental data. The flame front positions in RUN158 were shown in Figure 5. During the run-up phase, the flame arrivals were under estimated. Good agreements of flame front positions were obtained during the acceleration phase.

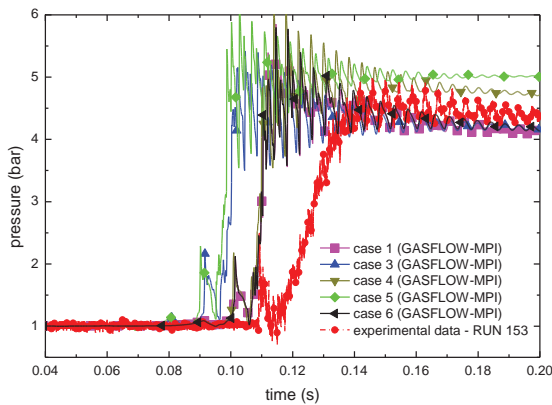


Figure 2. Pressure time evolution in RUN 153 during 0.04 s – 0.20 s

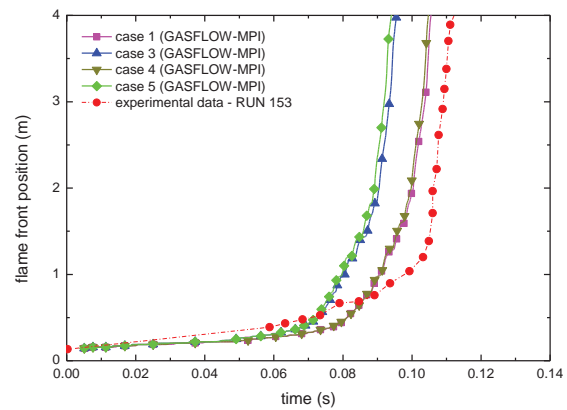


Figure 3. Turbulent flame propagation along the tube in RUN 153

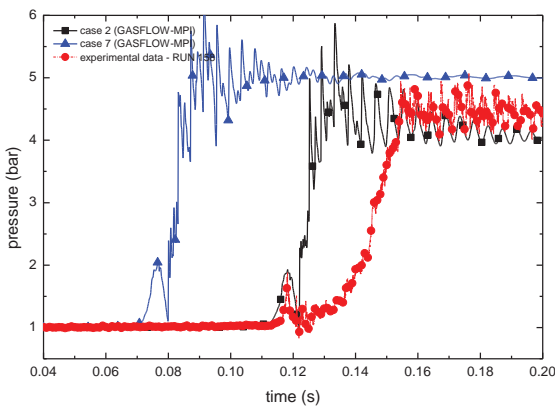


Figure 4. Pressure time evolution in RUN 158 during 0.04 s – 0.20 s

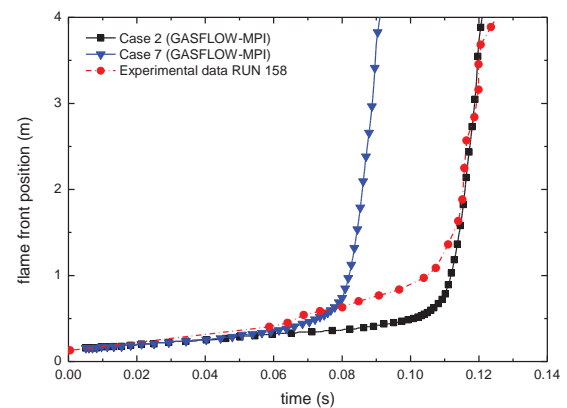


Figure 5. Turbulent flame propagation along the tube in RUN 158

It was found that the simulations during the acceleration phase were greatly influenced by the ignition volume, the ignition time duration, the initial turbulence intensity, and the turbulence intensity in the ignition volume. By using various combinations of these parameters, one can produce the low-speed acceleration phase with good results. However; the acceleration phase is not nearly as important in risk analysis as the fully turbulent flame propagation phase where the rate of pressure rise is high. For this reason, we often need to time-shift the fully turbulent results to coincide with the experiment.

#### 4.2. Effect of heat transfer modeling on pressure decay

After the combustion, the pressure decreases due to the heat losses. Condensation, convective and radiation heat transfer modeling are required to accurately predict the pressure decay. As illustrated in Figure 6, the pressure during 0.1 s ~ 0.2 s is constant and higher than the measured data in case 5 without heat transfer. For cases 1, 3, 4 and 6 in which various heat transfer mechanisms are involved, pressure can be observed to decay with various rates. It means the heat transfer start to play an important role at the very beginning after the combustion. The red dots represent the bandwidth of the measured pressure

history. With all heat transfer mechanisms turned on (case 1), the pressure decay rate agrees well with the measured data during 0.1 s ~ 0.5 s. However, the large measured pressure decay rate was not reproduced after 0.5 s. The measured pressure decays faster than the calculated results. One reason for this discrepancy could be thermal effects on the PCB pressure transducer, which are known to be very sensitive to heat transfer from burned gas. It is difficult to rule out the first possible reason since the details of the pressure measuring technics are absent. Another reason could be the deficits and uncertainties in the applied heat transfer models, such as the convective heat transfer coefficient, emissivity coefficient, effect of water film on the steam condensation and so on. The adequacy of the heat transfer modeling will be tested in the future by simulating other hydrogen combustion experiments in which temperatures of the heated wall were measured.

Figure 7 shows the total amount of energy integrated through the structures of the tube and dome with all three different ways of heat transfer in case 1. Since the surface area in the acceleration tube is very small compared to the dome, hardly any heat loss can be seen before 0.12 s in Figure 7. Steam condenses with a high rate during 0.12 s ~ 0.2 s after the combustion finishes. After 0.2 s, the steam condensation rate slows down. Regarding the radiation heat transfer, its effect becomes more significant with the time increasing which is due to the fact that the computed average steam temperature is still above 900 K at 1.0 s. The convective and radiation heat transfer dominates the heat losses of the combustion products during 0.12 s to 1.0 s, as the blue and red areas shown in Figure 7. In an experimental study of heat loss from the combustion products of turbulent flames and detonations in obstructed tubes by Kuznetsov, he concluded that instead of thermal radiation, convective heat transfer was the main mechanism of heat loss of the hydrogen flames [49]. It should be noted that Kuznetsov's study concerned detonations and the 50% of the total transferred energy was lost in around 10 ~ 20 ms due to convective heat transfer. In our study of deflagrations, the flame speed and temperature are much lower than the ones in detonation. The numerical results indicate that convective and radiation heat transfer mechanisms are the main contributors to the heat losses of the combustion products. However, the effects of steam condensation are not negligible. To increase the accuracy and reliability of the numerical simulations of hydrogen combustions, all mechanisms of heat transfer, including condensation, convective and radiation, should be considered.

The pressure time evolutions at PCB1 and total energy loss in RUN 158 are shown in Figure 8 and Figure 9. Again the measured pressure decay rate (red dots) is larger than the calculated ones in the long term after 0.3 s, even with all heat loss mechanisms turned on (case 2). The reasons could be the uncertainties of PCB sensor in pressure measurements after 0.2 s and the deficits in the numerical models. It is difficult to clarify in this paper since we have not sufficient knowledge about the measurement sensors. It seems that the calculated pressure decays and heat losses are independent of the blockage ratios, except that the thermal radiation has a slightly stronger impact on the heat loss in RUN 158 compared to RUN 153.

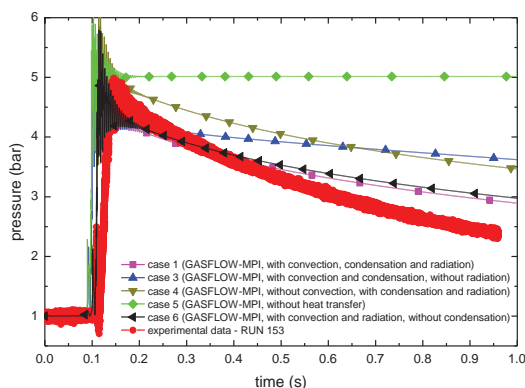


Figure 6. Pressure time evolution in RUN 153 during 0.0 s ~ 1.0 s

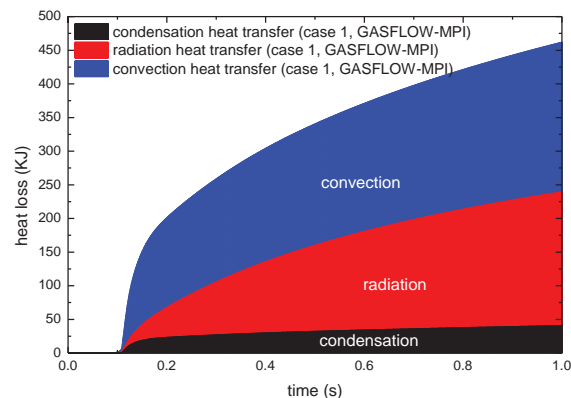


Figure 7. Total energy absorbed by the tube and dome in RUN 153 (case 1) during 0.0 s ~ 1.0 s

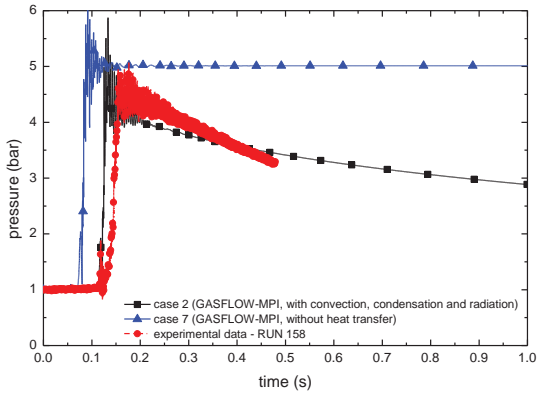


Figure 8. Pressure time evolution in RUN 158 during 0.0 s ~ 1.0 s

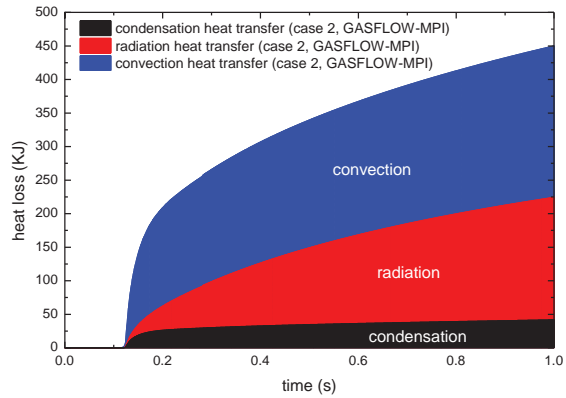


Figure 9. Total energy absorbed by the tube and dome in RUN 158 (case 2) during 0.0 s ~ 1.0 s

### 4.3. Effect of diluents

60 vol.% CO<sub>2</sub> and 40 vol.% He was used as diluents to serve as a simulant for steam. Three tests were conducted: 13 vol.% H<sub>2</sub> + 77 vol.% air + 10 vol.% diluents (case 8), 13 vol.% H<sub>2</sub> + 67 vol.% air + 20 vol.% diluents (case 9) and 13 vol.% H<sub>2</sub> + 57 vol.% air + 30 vol.% diluents (case 10). The calculated pressure time evolutions at PCB1 with various volume fractions of diluents are illustrated in Figure 10. The condensation, convective and radiation heat transfer models are switched on in the numerical simulations. The increase of diluents concentration leads to a smaller flame velocity (as expected) and an increase of the flame arrival time in the dome. The peak pressure is not very sensitive to the concentration of the diluents in the tested range (0-30 vol%), the maximum pressures decreases by about 10%. After combustion the pressure decreases with the same slope, which is independent of the diluent concentration.

Figure 11 shows the calculated effect of the diluents concentration on the flame position in the tube. Two different flame propagation regimes can be clearly distinguished in all three cases. A slow deflagration phase in the first 0.6 m of the tube, which contains no obstacles, and a fast deflagration phase in the section equipped with obstacles. The burning rate in GASFLOW-MPI seems to react somewhat more sensitive to the increased turbulence level from the obstacles than the experiment, but the general agreement with the experimental trend confirms the applied turbulent combustion model. The comparisons of the shifted calculated results and experimental data are also shown. Good agreement was obtained during the acceleration phase between the shifted results and the experimental data.

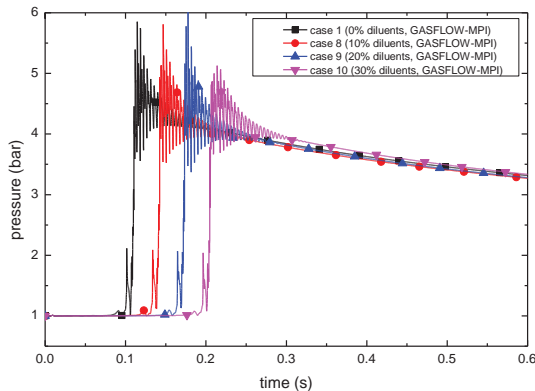


Figure 10. Effect of diluents on pressure time evolution during 0.0 s ~ 1.0 s

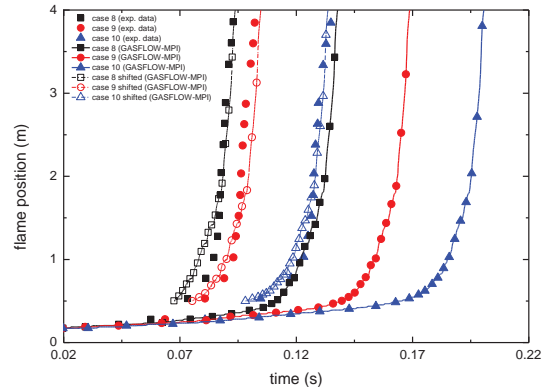


Figure 11. Effect of diluents on turbulent flame propagation along the tube

## 5. CONCLUSIONS

GASFLOW-MPI is a parallel semi-implicit pressure-based all-speed CFD code which solves the 3-D compressible Navier-Stokes equations in Cartesian or cylindrical coordinates using the proven algorithm of the Implicit Continuous Eulerian-Arbitrary Lagrangian-Eulerian (ICE'd-ALE) methodology. Our objective is to develop an integrated computational platform and achieve seamless simulations of the physical phenomena in geometrically complex NPP containments under severe accident, including thermal hydraulics, steam condensation and vaporization, chemical reactions, aerosol and liquid droplets behavior, fission product decay, hydrogen mitigation measures and so on.

Turbulent combustion models based on the transport equation of the density-weighted mean reaction progress variable have been recently developed and extended in GASFLOW-MPI code. The GASFLOW-MPI code has been validated using the SARNET-2 hydrogen deflagration experiments performed in the ENACCEF facility. It is shown that GASFLOW-MPI is capable of predicting the pressure increase rate, pressure peak, and the flame front position in the fast hydrogen deflagrations. The pressure decay can be reproduced by the GASFLOW-MPI with condensation, convective and radiation heat transfer models switched on shortly after the combustion (0.1 s ~ 0.5 s). Further investigations are needed for the predictions of pressure decay rate after 0.5 s, as shown in Figure 6 and Figure 8. It should be noted that the uncertainties and reliability in the long time measurements (> 0.5 s) of the pressure decay using PCB sensor require further clarification by the experimenters. For instance, what measures have been taken to control the known temperature sensitivity of PCBs? Since only the data at one transducer is available in the paper [32], it would also be good to see the measurements at other transducers to judge the measurement uncertainties.

Effect of various heat transfer mechanisms on the heat loss after the combustion was studied. It indicates that convective and radiation heat transfer mechanisms dominate the energy losses after the hydrogen deflagration. In order to increase the reliability of the numerical simulations, the heat loss due to steam condensation should be also considered. It is also found that the calculated run-up distance is sensitive to the volume of the ignition zone, the ignition time, and the initial values of turbulent intensities in the computational domain and ignition zone.

Further investigations and development are needed in order to improve combustion models predictability in GASFLOW-MPI, such as validated correlations for laminar and turbulence flame velocity. When the steam is condensed, thin water film will be formed at the inner surfaces of the tube and dome. The effect of thin water film on the heat loss and pressure decay needs further study.

## ACKNOWLEDGMENTS

The authors would like to thank Dr. Ahmed Bentaib for providing the data of SARNET-2 hydrogen deflagration experiments in the ENACCEF facility.

## REFERENCES

1. Containment Code Validation Matrix, NEA/CSNI/R(2014)3, May 2014.
2. Status Report on Hydrogen Management and Related Computer Codes, NEA/CSNI/R (2014) 8, June 2014.
3. J. Xiao, J. R. Travis, T. Jordan, P. Royle, G. A. Necker, R. Redlinger, and A. Svishchev, GASFLOW-III: A Computational Fluid Dynamics Code for Gases, Aerosols and Combustion, Volume 1: Theory and Computational Model, Karlsruhe Institute of Technology report, Revision 3.5, (2014).

4. J. Xiao, J. R. Travis, T. Jordan, P. Royl, G. A. Necker, R. Redlinger, and A. Svishchev, GASFLOW-III: A Computational Fluid Dynamics Code for Gases, Aerosols and Combustion, Volume 2: User's Manual, Karlsruhe Institute of Technology report, Revision 3.5, (2014).
5. C.W. Hirt., Amsden, A.A., and Cook, J.L., An Arbitrary Lagrangian-Eulerian Computing Method for All Flow Speeds, *J. Comp. Phys.* 14, 227, (1974).
6. F.H. Harlow, and A.A. Amsden, A numerical fluid dynamics calculation method for all flow speeds, *J. Comp. Phys.*, 8, p. 197, (1971).
7. P. Royl, C. Müller, J. R. Travis, T. Wilson, "Validation of GASFLOW for Analysis of Steam/Hydrogen Transport and Combustion Processes in Nuclear Reactor Containments," *Procs 13th Conference on Structural Mechanics in Reactor Technology*, Porto Alegre, RS, Brazil, (1995).
8. P. Royl, J. R. Travis, E. A. Haytcher, and H. Wilkening, "Analysis of Mitigating Measures during Steam/Hydrogen distributions in Nuclear Reactor Containments with the 3D Field Code GASFLOW," presented at the OECD/NEA CSNI Workshop on the Implementation of Hydrogen Mitigation Techniques, Winnipeg, Canada, (1996).
9. P. Royl, J. R. Travis, W. Breitung, "Benchmarking of the 3D CFD Code GASFLOW with Containment Thermal Hydraulic Tests from HDR and ThAI", *Procs IAEA-OECD CFD4NRS Conference*, (2006).
10. P. Royl, G. Necker, J. W. Spore, J. R. Travis, "3D Analysis of Hydrogen Recombination Experiments in the Battelle Model Containment with the GASFLOW Code." *Procs Jahrestagung Kerntechnik*, Munich, (1998).
11. P. Royl, J. R. Travis, W. Breitung, "Analyses of Containment Experiments with GASFLOW", *Procs Nureth-10 Conference*, Seoul, Korea, (2003).
12. H.J. Allelein, et al.: "International Standard Problem ISP-47 on Containment Thermal Hydraulics", *OECD -final report*, (2006).
13. P. Royl, J. R. Travis, W. Breitung, J. Kim, T. Kanzleiter, and S. Schwarz, "GASFLOW analysis of steam/hydrogen mixing with nitrogen in the OECD-NEA THAI HM-2 Benchmark," in *Proceedings of the NURETH 13*, Kanazawa, Japan, (2009).
14. J. Xiao, J. R. Travis, "How critical is turbulence modeling in gas distribution simulations of large-scale complex nuclear reactor containment?", *Annals of Nuclear Energy*, Volume 56, Pages 227–242, (2013).
15. J. Malet, Z. Parduba, S. Mimouni, J. Travis, "Achievements of spray activities in nuclear reactor containments during the last decade", *Annals of Nuclear Energy*, 74:134-142, (2014).
16. P. Royl, J. R. Travis, W. Breitung, J. Kim, and S. B. Kim, "GASFLOW Validation with Panda Tests from the OECD SETH Benchmark Covering Steam/Air and Steam/Helium/Air Mixtures", *Science and Technology of Nuclear Installations*, (2009).
17. J. Malet, S. Mimouni, G. Manzini, J. Xiao, L. Vyskocil, N.B. Siccama, R. Huhtanen, "Gas entrainment by one single French PWR spray, SARNET-2 spray benchmark", *Nuclear Engineering and Design*, Volume 282, Pages 44–53, (2015).
18. P. Royl, J. R. Travis, "Simulation of Hydrogen Transport with Mitigation Using the 3D Field Code GASFLOW", *Procs. 2nd International Conference on Advanced Reactor Safety*, Orlando, Florida, (1997).
19. P. Royl, J. R. Travis, W. Breitung, "Modelling and Validation of Catalytic Hydrogen Recombination in the 3D CFD Code GASFLOW II", *Procs IAEA-OECD CFD4NRS Conference Munich*, (2006).
20. S. Benz, P. Royl, S. Band, "Analysis of a hypothetical Loss of Coolant Accident in a Konvoi type NPP by GASFLOW and COCOSYS", *Procs Jahrestagung Kerntechnik*, Berlin, (2013).
21. H. Dimmelmeier, J. Eyink, M.A. Movahed, Computational validation of the EPR combustible gas control system. *Nuclear Engineering and Design* 249, 118–124, (2012).
22. P. Royl, W. Breitung, J. R. Travis, "Simulation of hydrogen transport with mitigation using the 3D field code GASFLOW", *Proceedings of the international topical meeting on advanced reactors safety: Vol. 1*, 578-588, (1997).
23. M. Heitsch, R. Huhtanen, Z. Téchy, C. Fry, P. Kostka, J. Niemi, B. Schramme, "CFD evaluation of hydrogen risk mitigation measures in a VVER-440/213 containment", *Nuclear Engineering and Design*, Vol. 240, pp. 385-396, (2010).
24. J. Kim, S. Hong, "Analysis of hydrogen flame acceleration in APR1400 containment by coupling hydrogen distribution and combustion analysis codes", *Progress in Nuclear Energy*, Volume 78, Pages 101–109, (2015).
25. J. Kim, "Hydrogen Safety Analysis of the OPR1000 Nuclear Power Plant during a Severe Accident by a Small-Break Loss of Coolant", *Proceedings of the KNS spring meeting*, (2009).
26. U. Lee, P. Royl, E. Seidelberger, G. Weimann, "Three Dimensional Analysis of the Steam-Hydrogen Distribution from a Hypothetical Small Break Severe Loss of Coolant Accident in a VVER 1000 Type reactor Containment Using GASFLOW II", *NURETH-10*, Seoul, Korea, (2003).
27. J. Xiong, Y. Yang, and X. Cheng, "CFD Application to Hydrogen Risk Analysis and PAR Qualification", *Science and Technology of Nuclear Installations*, Volume 2009 (2009)
28. J. Xiao, J.R. Travis, W. Breitung, T. Jordan, "Numerical analysis of hydrogen risk mitigation measures for support of ITER licensing", *Fusion Engineering and Design*, 85(2):205-214, (2010).

29. R. Zhang, X. Sun and Y. Dong, "The CFD Analysis of Hydrogen Behavior in HTR-PM during the Water ingress Accident Caused by Double-ended Guillotine Break of Two Steam Generator Heating Tubes", Proceedings of the 2014 22<sup>nd</sup> International Conference on Nuclear Engineering, Prague, Czech Republic, (2014).
30. T. Jordan, P. Royl, A. Kotchourko, A. Lelyakin, "Use of The KIT HYCODES System with a Conservative Source for the Simulation of Hydrogen Distribution and Combustion with/without Spray in a Large Break LOCA in the Korean APR1400", Jahrestagung Kerntechnik Berlin, (2015).
31. J. Xiao, J. R. Travis, P. Royl, A. Svishchev, T. Jordan and W. Breitung. "PETSC-Based Parallel Semi-Implicit CFD Code GASFLOW-MPI In Application Of Hydrogen Safety Analysis In Containment Of Nuclear Power Plant", Joint International Conference on Mathematics and Computation (M&C), Supercomputing in Nuclear Applications (SNA) and the Monte Carlo (MC) Method, Nashville, TN., April 19-23, (2015).
32. A. Bentaib, A. Bleyer, N. Meynet, N. Chaumeix, B. Schramm, M. Höhne, P. Kostka, M. Movahed, S. Worapittayaporn, T. Brählerf, H. Seok-Kang, M. Povilaitis, I. Kljenak, P. Sathiah, "SARNET hydrogen deflagration benchmarks: Main outcomes and conclusions", Annals of Nuclear Energy 74, 143–152, (2014).
33. B.E. Launder, B.I., Sharma, Application of the Energy-Dissipation Model of Turbulence to the Calculation of Flow Near a Spinning Disc, Letters in Heat and Mass Transfer, Vol. 1, No. 2, pp. 131-138, (1974).
34. N. Chakraborty and C. Stewart, Unsteady effects of strain rate and curvature on turbulent premixed flames in an inflow-outflow configuration, Combustion and Flame, 137(12), 129-147 (2004).
35. D. Veynante, and L. Vervisch, Turbulent combustion modeling, Progress in Energy and Combustion Science, 28(3), 193-266, 2002.
36. B. S. Brewster, S. M. Cannon, J. F. Farmer, F. Meng, Modeling of lean premixed combustion in stationary gas turbines, Progress in energy and Combustion Science, 25(4), 363-385 (1999).
37. N. Peters, Turbulent burning velocity for large-scale and small-scale turbulence, J. Fluid Mech., 384, 107-132 (1999).
38. V. L. Zimont, "Gas premixed combustion at high turbulence: turbulent flame closure combustion model", Experimental Thermal and Fluid Science, 21, 179-186, (2000).
39. V. L. Zimont, F. Biagioli, and K. Syed, "Modelling turbulent premixed combustion in the intermediate steady propagation regime", Progress in Computational Fluid Dynamics, 1, 14-28, (2001).
40. V. Zimont, W. Polifke, M. Bettelini, and W. Weisenstein. "An efficient computational model for premixed turbulent combustion at high reynolds numbers based on a turbulent flame speed closure". J. of Gas Turbines Power, 120:526–532, (1998).
41. A.N. Lipatnikov and J. Chomiak. "Turbulent flame speed and thickness: phenomenology, evaluation, and application in multi-dimensional simulations". Progress in Energy and Combustion Science, 28(1):1 74, (2002).
42. H. Schmid, P. Habisreuther and W. Leuckel, "A Model for Calculating Heat Release in Premixed Turbulent Flames", Combustion and Flame, 113, 79-91 (1998).
43. B. E. Launder and D. B. Spalding, "The numerical computation of turbulent flows", Comp. Meth. Appl. Mech. Eng., 3, 269 (1974).
44. R. B. Bird, W. E. Stewart, and E. N. Lightfoot, Transport phenomena, John Wiley and Sons, New York, (1960).
45. Gray, Kilham, and Müller, Heat Transfer from Flames, Elek Science, London (1976).
46. Hottel and Sarofim, Radiative Transfer, McGraw-Hill, New York (1967).
47. Rohsenow and Hartnett, Handbook of Heat Transfer, McGraw-Hill, New York (1973).
48. Taylor and Foster, The Total Emissivities of Luminous and Non-Luminous flames," Int. J. Heat Mass Transfer, Vol. 17, pp. 1591, (1974).
49. M. Kuznetsov, I. Matsukov and S. Dorofeev, "Heat loss rates from Hydrogen-Air turbulent flames in tubes", Combustion Science and Technology, Volume 174, Issue 10, (2002).